Diurnal and Semidiurnal Tides in Global Surface Pressure Fields

AIGUO DAI

National Center for Atmospheric Research, Boulder, Colorado*

JUNHONG WANG+

Program in Atmospheric and Oceanic Sciences, University of Colorado, Boulder, Colorado

(Manuscript received 21 September 1998, in final form 16 February 1999)

ABSTRACT

Global surface pressure data from 1976 to 1997 from over 7500 land stations and the Comprehensive Ocean–Atmosphere Data Set have been analyzed using harmonic and zonal harmonic methods. It is found that the diurnal pressure oscillation (S_1) is comparable to the semidiurnal pressure oscillation (S_2) in magnitude over much of the globe except for the low-latitude open oceans, where S_2 is about twice as strong as S_1. Over many land areas, such as the western United States, the Tibetan Plateau, and eastern Africa, S_1 is even stronger than S_2. This is in contrast to the conventional notion that S_2 predominates over much of the globe. The highest amplitudes (~1.3 mb) of S_1 are found over northern South America and eastern Africa close to the equator. Here S_1 is also strong (~1.1 mb) over high terrain such as the Rockies and the Tibetan Plateau. The largest amplitudes of S_2 (~1.0–1.3 mb) are in the Tropics over South America, the eastern and western Pacific, and the Indian Ocean. Here S_1 peaks around 0600–0800 LST at low latitudes and around 1000–1200 LST over most of midlatitudes, while S_2 peaks around 1000 and 2200 LST over low- and midlatitudes. Here S_1 is much stronger over the land than over the ocean and its amplitude distribution is strongly influenced by landmasses, while the land–sea differences of S_2 are small. The spatial variations of S_1 correlate significantly with spatial variations in the diurnal temperature range at the surface, suggesting that sensible heating from the ground is a major forcing for S_1. Although S_2 is much more homogeneous zonally than S_1, there are considerable zonal variations in the amplitude of S_2, which cannot be explained by zonal variations in ozone and water vapor. Other forcings such as those through clouds' reflection and absorption of solar radiation and latent heating in convective precipitation are needed to explain the observed regional and zonal variations in S_2. The migrating tides S_2^1 and S_2^2 predominate over other zonal wave components. However, the nonmigrating tides are substantially stronger than previously reported. The amplitudes of both the migrating and nonmigrating tides decrease rapidly poleward with a slower pace at middle and high latitudes.

1. Introduction

Of the 342 W m^{-2} of solar radiation reaching the top of the atmosphere, about 168 W m^{-2} are absorbed by the earth's surface and 67 W m^{-2} are absorbed by the atmosphere (43 W m^{-2} by water vapor, 14 W m^{-2} by ozone, 7 W m^{-2} by clouds, and 3 W m^{-2} by O_2 and CO_2) (Kiehl and Trenberth 1997). This atmospheric solar heating, combined with upward eddy conduction of heat from the ground, generates internal gravity waves in the atmosphere at periods of the integral fractions of a solar day (primarily at the diurnal and semidiurnal periods). These waves cause regular oscillations in atmospheric wind, temperature, and pressure fields, which are often referred to as atmospheric tides (Wallace and Hartranft 1969; Chapman and Lindzen 1970; Haurwitz and Cowley 1973; Hsu and Hoskins 1989; Whiteman and Bian 1996). Due to the fact that 24 hours are longer than the local pendulum day (the period corresponding to the local Coriolis parameter) poleward of 30° lat, the diurnal tide is incapable of propagating vertically over these regions to reach the ground (Lindzen 1967). Although the diurnal tide is often suppressed at the ground, its amplitude in the upper atmosphere is comparable with, and may be much larger than, the semidiurnal tide.

In the surface pressure field, the semidiurnal oscillation S_2 is thought to predominate over much of the globe, and is regularly distributed in its amplitude (which is about 1 mb in the Tropics and decreases poleward) and phase (S_2 usually peaks 2–3 h before noon

* The National Center for Atmospheric Research is sponsored by the National Science Foundation.

+ Current affiliation: National Center for Atmospheric Research, Boulder, Colorado.

Corresponding author address: Dr. Aiguo Dai, NCAR, P.O. Box 3000, Boulder, CO 80307-3000.
E-mail: adai@ucar.edu

and midnight). The classic tidal theory (Chapman and Lindzen 1970) predicts that solar heating through ozone explains about two-thirds of S_2's amplitude while water vapor and heating from the ground account for the rest. Oscillation S_2 is dominated by its wavenumber 2 mode S_2^2 (moving westward at the speed of the mean sun) (Haurwitz and Cowley 1973). In contrast to S_2, the diurnal oscillation S_1 in the surface pressure field is very irregularly distributed and is influenced strongly by landmasses. Water vapor heating provides a much larger contribution to S_1 than ozone heating (Groves and Wilson 1982). Locally, diurnal temperature and wind variations can greatly increase the amplitude of S_1.

Model calculations with more recent ozone and water vapor heating profiles suggest that additional heating is needed in order to explain the observed amplitude of S_1 and S_2 (Groves and Wilson 1982; Braswell and Lindzen 1998). Forbes and Garrett (1979) suggested that nonmigrating tides (which depend on both local time and longitude) could be excited by orographic features and longitudinal variations in water vapor and ozone. Model simulations suggest that the upward sensible heat flux from the ground due to solar heating contributes significantly to the nonmigrating components of S_1 (Tsuda and Kato 1989). The migrating component (which is a function of local time) of S_1 is underestimated by more than one-third by the classic tide theory even with the updated ozone and water vapor heating (Braswell and Lindzen 1998). The latent heating associated with convective precipitation, which has a strong diurnal cycle (Dai et al. 1999a), was found to be important mostly for S_2 (Lindzen 1978). It is suggested that the recently debated anomalous solar absorption by clouds or water vapor, which is not included in the radiation fluxes from Kiehl and Trenberth (1997) cited above, could significantly reduce this gap between the theory-predicted and the observed S_1 (Braswell and Lindzen 1998).

Besides heating, there is also a mass forcing on surface pressure tides resulting from the imbalance between evaporation and precipitation, which is significant globally on seasonal timescales (about 0.2 mb) (van den Dool and Saha 1993; Trenberth and Guillemot 1994). We know that evaporation peaks during the day (at least over the land), while precipitation occurs more frequently during early morning over the ocean (Janowiak et al. 1994) and in the afternoon over many land areas (Dai et al. 1999a). As the sun moves over the oceans (land), global evaporation is likely to increase (decrease). These diurnal variations are likely to induce a diurnal cycle of net water flux at the surface, which could provide an additional forcing for surface pressure tides. However, we are unaware of any studies addressing this mass forcing.

Because the longitude-dependent nonmigrating diurnal tides are nonnegligible at the surface and mixed up with the migrating tides, the migrating tides can be determined only from data around a latitude circle (Lindzen 1979). Most of our observational knowledge of S_1 and S_2 on a global scale comes from the analyses of surface pressure data from about 250 stations done by Haurwitz et al. from the 1950s to the early 1970s (Haurwitz 1956; Haurwitz 1965; Haurwitz and Cowley 1973). A majority of these stations were located in western Europe and North America while only about 50 of them were in the Southern Hemisphere. Most of the open oceans were not covered at all in these analyses. Obviously, the global distributions of S_1 and S_2 and their seasonal variations derived from such a limited spatial coverage should be interpreted with caution. Furthermore, the sparse spatial sampling and coarse grid resolution (15° long by 10° lat) used by Haurwitz and Cowley (1973) make their results of wave components likely to be unreliable, especially at high wavenumbers. Nevertheless, the S_1 and S_2 maps and their main wave components from these analyses have been widely cited and applied in the literature (e.g., Tsuda and Kato 1989; Lindzen 1990; Whiteman and Bian 1996; Deser and Smith 1998; Braswell and Lindzen 1998). Hamilton (1980a) updated Haurwitz's dataset by adding 35 new stations (only two of them in the Southern Hemisphere). Regional analyses of S_1 and S_2 (e.g., Trenberth 1977; Mass et al. 1991; Kong 1995) revealed more small-scale features. More recent efforts to document global variations of S_1 and S_2 by analyzing the European Centre for Medium-Range Weather Forecasts analysis (Hsu and Hoskins 1989) and National Centers for Environmental Prediction (NCEP) reanalysis (van den Dool et al. 1997) 6-hourly data were hampered by the coarse temporal resolution of the data as well as the deficiencies of the models.

In this study, we update the earlier analyses and document S_1 and S_2 on a global scale by analyzing 3-hourly surface pressure data from 1976 to 1997 from all the land and ocean weather stations included in the Global Telecommunication System (GTS) and the marine reports from the Comprehensive Ocean–Atmosphere Data Set (COADS). There are about 15 000 stations included in GTS, but only 4000–7000 stations report at any given time, which still provides good spatial coverage over all the continents and islands except the Antarctic. The COADS data include most of the reports from commercial ships and various kinds of buoys and provide fairly good coverage of the global oceans during the 1976–97 period. We also analyzed the 3-hourly surface pressure data from 1980 to 1994 from the reanalysis with version 1 of the Goddard Earth Observing System (GEOS-1) Data Assimilation System (DAS) and found that the amplitudes of S_1 and S_2 of the reanalysis data tend to be smaller in high latitudes and larger in low latitudes than observed. We applied harmonic analysis to derive the amplitudes and phases of S_1 and S_2, and zonal harmonic analysis (Haurwitz and Cowley 1973) to decompose S_1 and S_2 into various zonal wave components. We also compared the geographical and seasonal patterns of S_1 and S_2 with those of atmospheric total column ozone, atmospheric precipitable water, and

sensible heat flux from the earth's surface [which is approximated by the mean diurnal range of surface air temperature (DTR)]. We find that spatial variations in the amplitude of S_1 are strongly correlated with DTR, suggesting that sensible heat flux is a major forcing for S_1 over land areas.

In section 2, we describe the datasets used in this study. Harmonic and zonal harmonic analysis methods are described in section 3. The global distributions of S_1 and S_2, their seasonal variations, and zonal wave components are presented and compared with earlier studies in section 4. In section 5 we compare the seasonal and spatial patterns of S_1 and S_2 with those of atmospheric total column ozone, atmospheric precipitable water, and DTR. A summary is given in section 6.

2. Data

The 3-hourly surface pressure data were extracted from the GTS synoptic weather reports archived at the National Center for Atmospheric Research (NCAR) (DS464.0; http://www.scd.ucar.edu/dss/datasets/ds464.0.html). This surface dataset, which covers the time period from July 1976 to April 1997 and has a volume of about 2.5 GB per year, contains 3-hourly (0000, 0300, 0600 UTC, etc.) surface pressure measurements from about 15 000 land and ocean stations and 6-hourly marine reports from commercial ships and buoys. Because the spatial coverage of this dataset is poor over the equatorial Pacific and the southern oceans, we also processed individual marine reports from the COADS dataset (Woodruff et al. 1993) from January 1976 to December 1995 (data after 1995 had not been released at the time of analysis). The COADS reports include hourly data from a small number of buoys and 6-hourly and 3-hourly data from ships and buoys. We used the COADS reports at the GTS 3-hourly reporting times (i.e., 0000, 0300, 0600 UTC, etc.). The number of reports of surface pressure at 0300, 0900, 1500, and 2100 UTC is generally less than that at 0000, 0600, 1200, and 1800 UTC for both the GTS and COADS datasets, especially over the southern oceans in the COADS data.

In contrast to the fixed land stations, the ships and many of the buoys are moving and thus their reports do not have a fixed long–lat location. Thus, we averaged individual marine reports within each 2.5° long by 2° lat box to obtain a mean value for each grid box at each reporting time. Land and fixed ocean stations were analyzed individually for the amplitude and phase of S_1 and S_2, which were then combined with those from the gridded marine data. The amplitude and phase were further gridded onto a 5° long × 4° lat grid using the natural neighbor interpolation method (Watson 1994). The gridded amplitudes and phases were then used in the plotting and zonal harmonic analysis.

Over the southern oceans (i.e., south of about 50°S) and some parts of the central equatorial Pacific, surface pressure data are available only at 0000, 0600, 1200, and 1800 UTC. These 6-hourly marine reports are not sufficient for sampling the semidiurnal cycle. Previous analyses (e.g., Haurwitz and Cowley 1973) and the 3-hourly GEOS-1 reanalysis data (which have a global coverage) indicated that relative to local time the semidiurnal cycle does not change rapidly in the longitudinal direction over the oceans. This allowed us to use reports (after the daily mean is removed) 10° to the east (40 min later) and to the west (40 min earlier) to supplement the 6-hourly data at some (~15%) of the ocean grid boxes (away from coastlines). This resulted in 12 reports per day (0000, 0040, 0520, 0600, 0640 UTC, etc.) at these ocean boxes. Sampling tests with given diurnal and semidiurnal harmonics showed that the 3-hourly even sampling (i.e., 0000, 0300, 0600 UTC, etc.) and the supplemented 12 reports day^{-1} sampling are sufficient to exactly reproduce the original harmonics.

The individual observations at each synoptic hour were averaged over each season (DJF = December–February, MAM = March–May, JJA = June–August, and SON = September–November) for each year. For the seasonally averaged values to be used in our harmonic analysis, we required at least seven of the eight synoptic hours to have data for the land stations and eleven of the twelve supplemented synoptic hours to have data for the marine boxes. About 7500 GTS stations meet this requirement with 4 or more yr of data during the 1976–97 period. Of the stations, about 4500 stations have at least 10 yr of data during the period. GTS stations and the ocean grid boxes with less than 4 yr of data were excluded from our analysis. Mass et al. (1991) showed that over the United States using more than 4 yr of data did not change the results of S_1 and S_2. The stations and ocean boxes with sufficient data that were used in our analysis are shown in Fig. 1. It can be seen that the station and marine observations provide good coverage over the globe except for the Antarctic, the Arctic Ocean, and the southern Pacific (south of 52°S and 70°–180°W) where the data are sparse. Given the relatively large-scale nature of S_1 and S_2, the spatial coverage of Fig. 1 should be sufficient for capturing the large-scale (>500 km) features of S_1 and S_2, especially over the Northern Hemisphere.

The annual-mean surface pressure data (expressed as anomalies relative to daily mean values) used to derived annual S_1 and S_2 are shown in Fig. 2. It can be seen that the westward-propagating wavenumber 2 mode predominates over low and middle latitudes but becomes less evident at high latitudes. The anomalies are largest over South America and Africa. Figure 2 is qualitatively consistent with the global patterns in the semidiurnal component of atmospheric pressure velocity ω (Trenberth et al. 1995), assuming that ω represents vertical motion of the air.

The station and marine data of surface pressure potentially contain various errors. For example, the surface pressure data are resolved to the nearest 0.1 mb, which is a substantial fraction of the amplitudes of S_1 and S_2

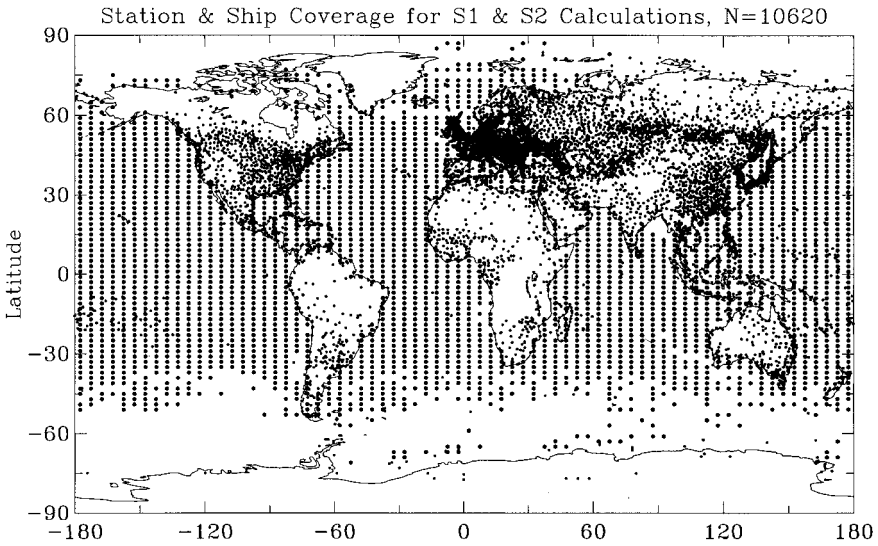

FIG. 1. Locations of the 7537 stations (small dots) and 3083 ocean boxes (big dots) with 4 or more yr of surface pressure data during the 1976–97 period that are used for annual S_1 and S_2 calculations (the coverage for each season is similar). About 4500 of the stations and 2630 of the ocean boxes have 10 or more yr of data during the period. Negative (positive) latitudes indicate the Southern (Northern) Hemisphere.

(about 1 mb at low latitudes and 0.2–0.5 mb at high latitudes). However, the measurement errors are likely to be random and thus are significantly reduced after averaging over the seasons and the 22-yr period. Another error may result from changes in barometers. Cooper (1984) shows that the amplitudes of the pressure tides may change by up to 20% due to changes in mercury barometers mainly because different barometers have different temperature corrections. Both mercury and aneroid barometers are used at land stations and on ships. It will be very difficult, if possible at all, to quantify the systematic errors associated with various types of barometers in all the station and marine records. We will compare our results to those based on the data before the 1970s when mercury barometers were often used. Furthermore, the phase estimated from the relatively coarse temporal sampling (3-h interval) will have an uncertainty up to ± 1.5 h. In our analysis temporal averaging and spatial smoothing were applied to emphasize the mean large-scale features. It is likely that the maximum amplitudes shown in this study may be lower than those at individual stations because of the smoothing used in contouring.

Because of its global coverage, especially over the oceans, we also analyzed the 3-hourly averaged surface pressure dataset from the reanalysis with the GEOS-1 DAS (Wu et al. 1997). This monthly dataset covers the period from 1980 to 1994 and is on a $2.5° \times 2°$ global grid. While the data assimilation model incorporates surface observations, the model itself has a significant influence on the assimilated surface pressure field. Since the pressure data are averaged over a 3-h period, the calculated amplitudes of S_1 and S_1 need to be multiplied by a factor (F) to obtain the real amplitudes that one would get from using instantaneous values (such as from the station data). The factor $F = \omega\Delta t/[2 \sin(\omega\Delta t/2)]$ where ω = angular frequency and Δt = averaging time period ($=3$ h), can be easily derived by averaging a sine function over a given period. Here $F = 1.0262$ for S_1 and 1.1107 for S_2, with $\omega = 2\pi/24$ for S_1 and $2\pi/12$ for S_2.

3. Analysis methods

We applied harmonic and zonal harmonic analyses to extract the solar diurnal and semidiurnal oscillations from the surface pressure data. We followed the analysis procedure described by Haurwitz and Cowley (1973). The surface pressure data at each location are represented by

$$P(t') = P_0 + S_1(t') + S_2(t') + \text{residual} \quad (1)$$

$$S_n(t') = A_n \sin(nt' + \sigma_n) = a_n \cos(nt') + b_n \sin(nt'), \quad n = 1, 2, \quad (2)$$

where P_0 is the daily mean pressure, A_n is the amplitude (note: the peak-to-peak amplitude is $2A_n$), σ_n the phase, t' local mean solar time (LST) expressed in degrees or radians (i.e., $t' = 2\pi t_1/24$, where t_1 is LST in hours). The 3-hourly station data and the supplemented marine data are insufficient for resolving harmonics with periods shorter than 12 h. Although accurate estimates of these high-order harmonics are not available over most of the globe, some analyses of hourly data showed that these high-order harmonics (primarily S_3) are much (at least a factor of 4–5) smaller than S_1 or S_2 (Trenberth

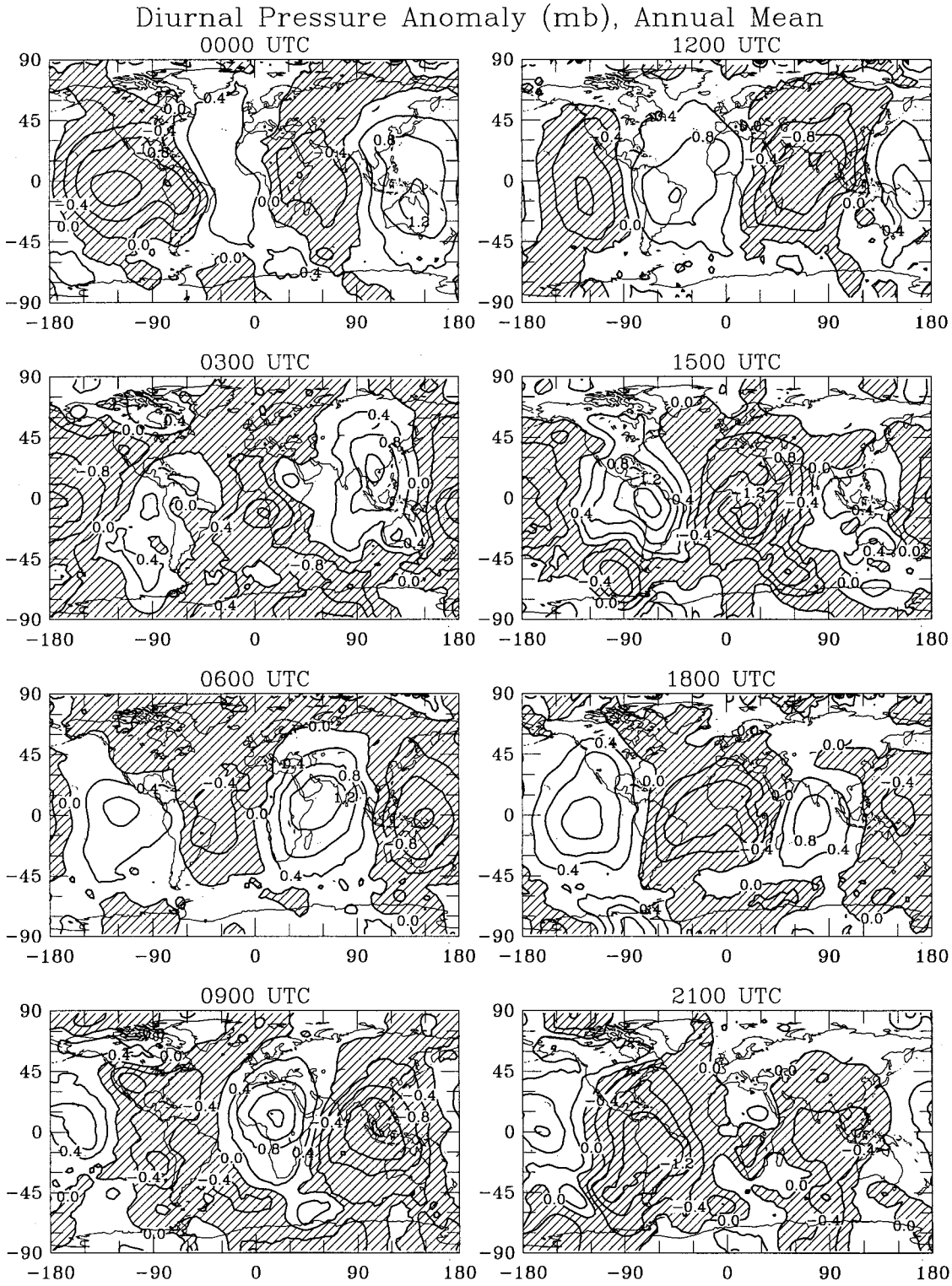

FIG. 2. Annual-mean surface pressure anomalies (mb) relative to daily mean values at the 3-hourly observation times derived by averaging and gridding the station and marine pressure data of the 1976–97 period. Negative values are hatched. Contour interval is 0.4 mb. Plots for seasonal mean pressure are similar.

1977; Cooper 1984; Mass et al. 1991). Therefore, the error induced by the aliasing of the high-order harmonics is likely to be small ($\leq$10% over most areas) in Eqs. (1) and (2).

The harmonic coefficients a_n and b_n are then interpolated onto a 5° long × 4° lat grid using the natural neighbor interpolation method (Watson 1994). At each latitude θ, the gridded coefficients are then expanded using trigonometric series of the longitude λ (which is zero at Greenwich and increases eastward)

$$a_n(\lambda, \theta) = \sum_{\nu=0}^{\infty} k_n^{\nu} \cos(\nu\lambda) + l_n^{\nu} \sin(\nu\lambda) \quad (3)$$

$$b_n(\lambda, \theta) = \sum_{\nu=0}^{\infty} q_n^{\nu} \cos(\nu\lambda) + r_n^{\nu} \sin(\nu\lambda), \quad (4)$$

where the k_n^{ν}, l_n^{ν}, q_n^{ν}, and r_n^{ν} depend on θ. Substituting Eqs. (3) and (4) into (2), replacing t' with Greenwich mean time (GMT) $t = t' - \lambda$, after some trigonometric transformations (2) becomes (Haurwitz and Cowley 1973)

$$S_n(t) = \sum_{s=-\infty}^{\infty} [a_n^s \cos(nt + s\lambda) + b_n^s \sin(nt + s\lambda)] \quad (5)$$

$$a_n^s = \frac{1}{2}(k_n^{n-s} + r_n^{n-s}), \qquad b_n^s = \frac{1}{2}(q_n^{n-s} - l_n^{n-s}), \quad \text{for } s < n \quad (6)$$

$$a_n^s = \frac{1}{2}(k_n^{s-n} - r_n^{s-n}), \qquad b_n^s = \frac{1}{2}(q_n^{s-n} + l_n^{s-n}), \quad \text{for } s > n \quad (7)$$

$$a_n^s = k_n^0, \qquad b_n^s = q_n^0, \quad \text{for } s = n. \quad (8)$$

Waves with wavenumber s are referred to as S_n^s. In particular, waves with $s = n$ travel westward at the speed of the mean sun. When expressed in local mean time t', these waves are independent of longitude and called migrating tides. The waves with $s \neq n$ depend on both local time and longitude and are called nonmigrating tides.

The amplitude, $A_n^s(\theta) = [(a_n^s)^2 + (b_n^s)^2]^{1/2}$, of the waves with large positive or negative wavenumbers is sensitive to the regional features in the gridded a_n and b_n fields. Our tests showed that in general the higher the resolution used in the gridding (which is limited by the spatial sampling of the data), the larger the amplitude at the high wavenumbers. Based on the spatial coverage of the data, we used a resolution of 5° long by 4° lat, which effectively smooths out variations on scales less than about 500 km. A global mean amplitude, $\overline{A}_n^s = \Sigma_\theta [A_n^s(\theta) \cos\theta]/\Sigma_\theta \cos\theta$ (Haurwitz and Cowley 1973), is computed for each wavenumber and is used to evaluate which wave components are important for S_1 and S_2 on a global scale.

4. Results

a. The solar diurnal oscillation, S_1

1) Global distributions of amplitude and phase

Figure 3 shows the global distribution of the amplitude of S_1 in the mean DJF, JJA, and annual pressure averaged over the 1976–97 period. It can be seen that the amplitude of S_1 is generally much larger over the land than over the ocean, especially at low latitudes (where solar heating is strong), over high terrain such as the western United States and the Tibetan Plateau, and in deserts such as northern Africa and central Australia. This results in large gradients in amplitudes across coastal areas where contour lines are approximately parallel to coastlines. This is consistent with the large diurnal variations of surface winds (such as land–sea breezes) around coastlines (Dai and Deser 1999). The largest amplitudes (~1.3 mb, much larger at some individual stations) for mean annual pressure are located over northern South America and eastern Africa close to the equator. The next largest amplitudes (~1.1 mb) are over the Rocky Mountains and the Tibetan Plateau. Over the open oceans, the amplitude ranges from 0.3 to 0.6 mb and does not decrease monotonically poleward, contrary to Haurwitz and Cowley's (1973) findings. Haurwitz and Cowley's data included only a few island stations and no marine reports. In fact, there seems to be a secondary maximum zone of S_1 around 60°S (45°S in JJA) where the amplitude reaches 0.5–0.7 mb, although the results south of about 50°S are less reliable because of the sparse observations there (cf. Fig. 1). Similar patterns were found for the diurnal harmonics of sea level pressure.

The differences between the DJF and JJA amplitudes of S_1 are large over many land areas. For example, the amplitude over central Australia is about 0.9–1.1 mb in DJF, compared with about 0.6–0.7 mb in JJA. The geographic distribution of the JJA minus DJF amplitude difference suggests that the seasonal, meridional movement of the maximum solar heating zone or the intertropical convergence zone (ITCZ) is the main cause for seasonal variations of S_1. For example, as the ITCZ moves into the Northern Hemisphere in JJA over the Indian Ocean and the western Pacific, the amplitudes of S_1 in northern subtropics and midlatitudes increases to their local annual maxima. On the other hand, during DJF the amplitudes peak locally over southern South America, southern Africa, and southern and central Australia as the zonal maximum solar heating moves into the Southern Hemisphere. In general, seasonal variations over the oceans are small. The amplitude maps of MAM and SON are similar to the annual.

While Haurwitz and Cowley (1973) also obtained large amplitudes of S_1 comparable to Fig. 3 over South America, Africa, the southwestern United States, and the Tibetan Plateau, their location of the centers differs

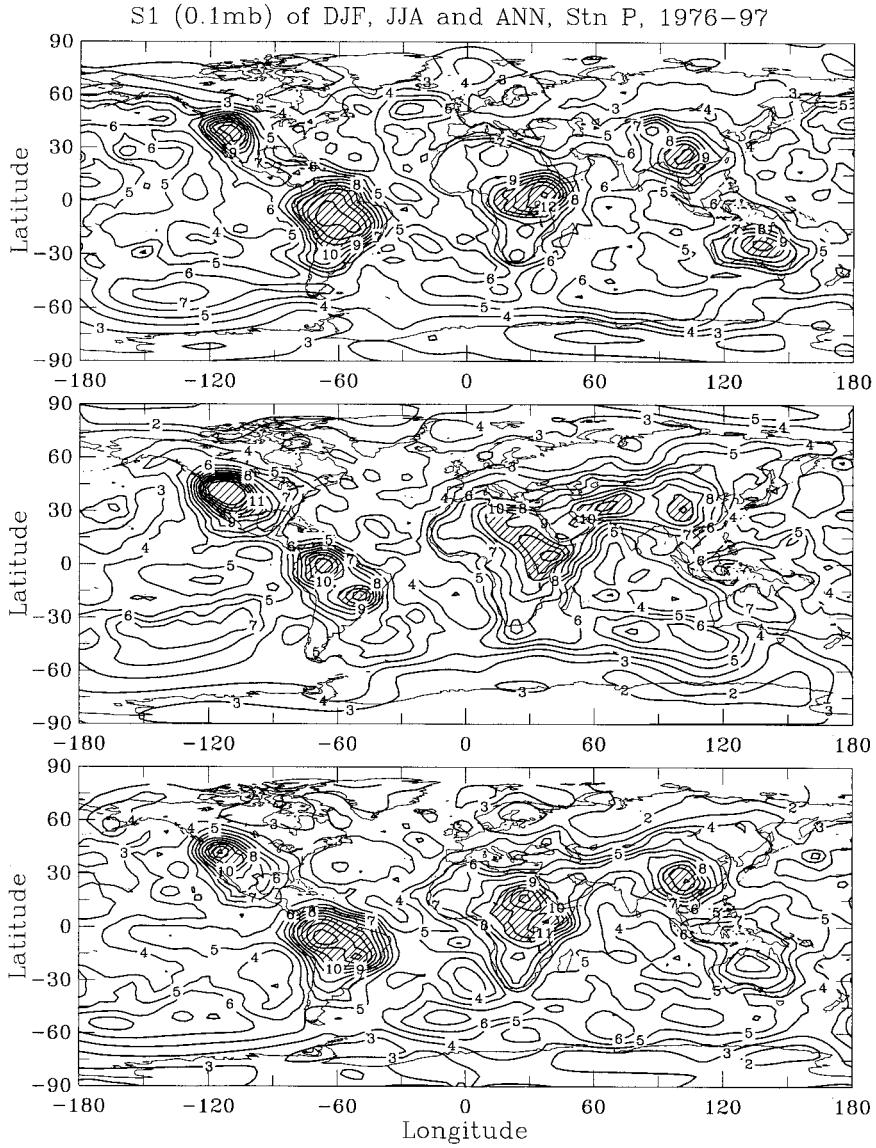

FIG. 3. Amplitude (in units of 0.1 mb) of the diurnal oscillation, S_1, in mean DJF (top panel), JJA (middle panel), and annual (bottom panel) surface pressure. Values over 1.0 mb are hatched. Contour interval is 0.1 mb.

substantially from Fig. 3. For example, the high-amplitude center over North America extends from the southwestern United States to northern Mexico in Haurwitz and Cowley's (1973) results, while it is confined mostly to the western United States in Fig. 3. These differences likely result from the poor station coverage over these regions in Haurwitz and Cowley's (1973) work (e.g., there were only 5–6 stations from the Rockies to Mexico and no stations in northern and central South America except a few on the eastern coast). The magnitude and regional patterns of the amplitudes shown in Fig. 3 are consistent with (although slightly lower due to smoothing than) those of Trenberth (1977) over New Zealand, Mass et al. (1991) over the United States, and Kong (1995) over Australia.

Figure 4 shows the phase (reported as T_{max}, the local time when the S_1 maximum occurs) of S_1 for annual surface pressure; plots for seasonal S_1 are similar. It can be seen that the land–sea differences in the phase are small, in contrast to the distribution of the amplitudes. Over low latitudes (30°S–30°N), S_1 reaches maxima in the morning around 0600–0800 LST (phase σ_1 = 0°∼−30°). In both northern and southern midlatitudes, S_1 peaks in the late morning around 1000–1200 LST (σ_1 = 300°∼270°), except in eastern Asia and the North Pacific where T_{max} is around 0600–0800 LST. This is in

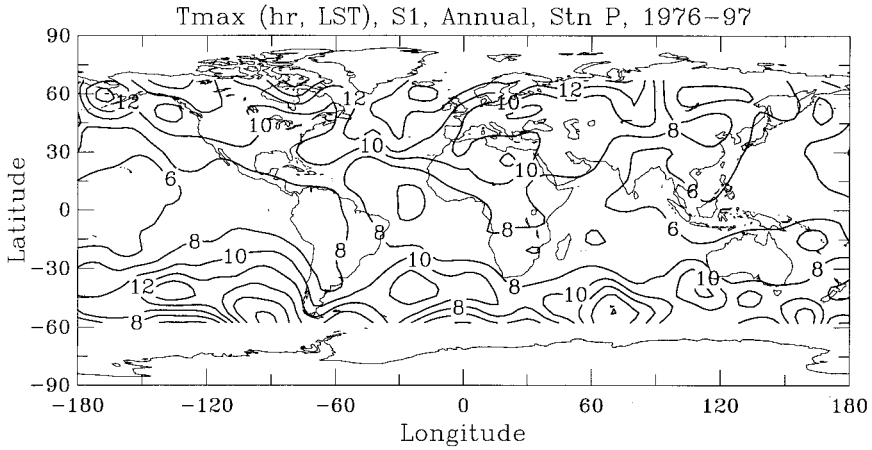

FIG. 4. Local solar time T_{max} (h) when the diurnal oscillation, S_1, of annual surface pressure reaches its maximum. Here S_1 is represented by $S_1 = A_1 \sin(2\pi t/24 + \sigma_1)$, where A_1 is the amplitude shown in Fig. 3, t local solar time in hours, and phase $\sigma_1 = \pi/2 - 2\pi T_{max}/24$.

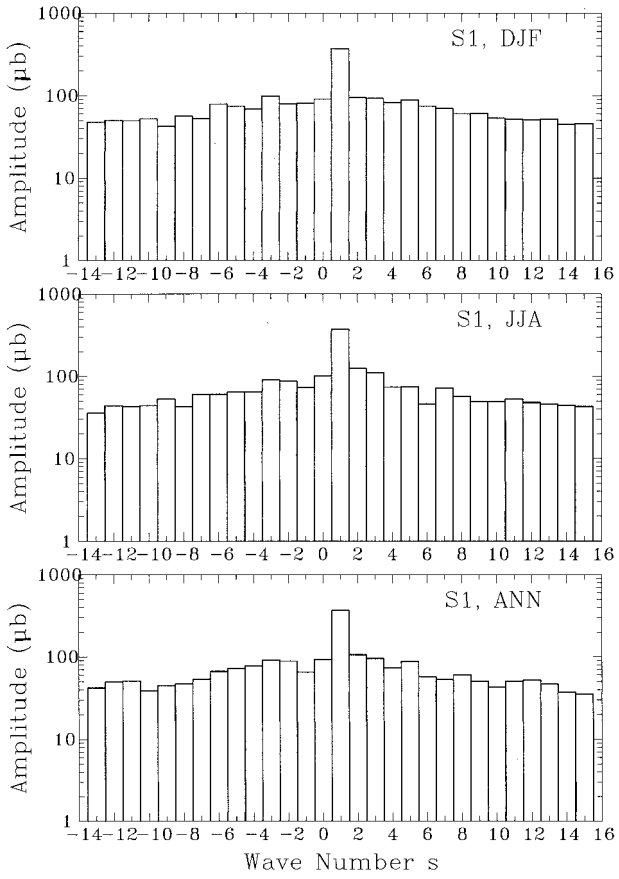

FIG. 5. Globally averaged amplitudes (μb) of S_1 at various wave components for mean DJF (top panel), JJA (middle panel), and annual (bottom panel) surface pressure.

contrast to Haurwitz and Cowley's (1973) findings where the maximum of S_1 tends to occur in midlatitudes about 90 min earlier in the Southern Hemisphere than in the Northern Hemisphere. Trenberth (1977) reported a phase of about $+30°$ to $-30°$ (or T_{max} = 0400–0800 LST) over New Zealand for annual S_1, which is similar to that shown in Fig. 4. Mass et al. (1991) found a T_{max} of about 0700 LST for S_1 over the United States, which is about 1–2 h earlier than that shown in Fig. 4. Kong (1995) showed a phase of 360°–320° (or T_{max} = 0600–0840 LST) over Australia, which is in good agreement with Fig. 4. Van den Dool (1997) found a T_{max} of 0500–0600 LST around the equator, which is consistent with Fig. 4, although there are more zonal variations in Fig. 4. It should be pointed out that the phase estimated from station data can vary considerably from one station to another on small scales (Trenberth 1977) and the error bars are likely to be large [note that σ_1 is estimated based on $\tan^{-1}(a_1/b_1)$ from Eq. (2)]. Figure 4 shows only the large-scale patterns of the phase.

2) ZONAL WAVE COMPONENTS

Figure 5 shows the globally averaged amplitudes for wave components at wavenumber $s = -14$ to $+15$ for DJF, JJA, and annual S_1. The wavenumber 1 component, S_1^1, has a global mean amplitude of about 370 μb (1 μb $= 10^{-3}$ mb), whereas the next closest amplitude (S_1^2) is about 100 μb. The amplitudes at higher wavenumbers decrease very slowly. We found that low grid resolution and smoothing used in deriving S_1 can significantly reduce the high wavenumber components and enhance S_1^1 (same is true for S_2 where the main component is S_2^2). The seasonal differences in the wave components are small.

Haurwitz and Cowley (1973) showed a global mean amplitude of about 410 μb for annual S_1^1 and much lower amplitudes ($\approx$20–30 μb) at the high ($s \leq -4$ and $s >$

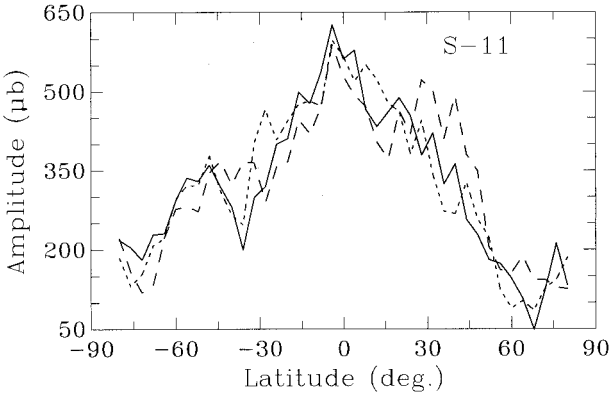

FIG. 6. Latitudinal distribution of the amplitude (μb) of S_1^1 (wavenumber 1 component of S_1) of mean DJF (short broken line), JJA (long broken line), and annual (solid line) surface pressure.

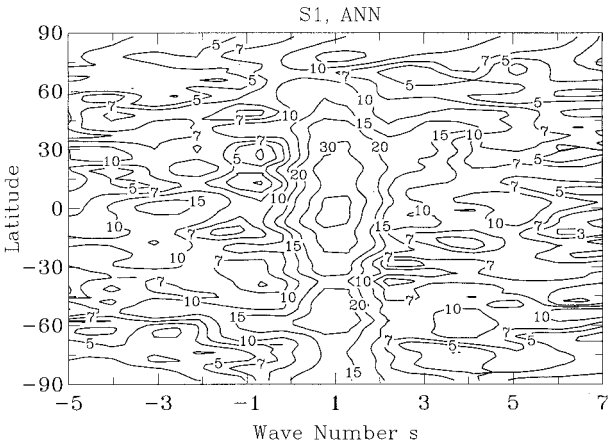

FIG. 7. Latitudinal distribution of the amplitude (μb) of S_1 at various wavenumbers.

6) wavenumbers. Also, S_1^{-3} is not much stronger than the adjacent ones, in contrast to Haurwitz and Cowley's (1973) findings. These differences are expected because Haurwitz and Cowley (1973) used a much coarser grid (15° long by 10° lat), which cannot adequately resolve the higher components.

The amplitude of the main wave S_1^1 for annual pressure is about 626 μb at about 4°S and decreases rapidly to the north and south (Fig. 6), with a slower pace in northern subtropics and a secondary peak around 48°S. Oscillation S_1^1 is weaker in JJA than in DJF over low latitudes and southern midlatitudes, but stronger in JJA than in DJF north of about 20°N, which is consistent with the seasonal differences shown in Fig. 3.

Haurwitz and Cowley (1973) used $\cos^3\theta$ to represent the latitudinal dependence of the amplitude of S_1^1. We found that $\cos^3\theta$ or higher-order polynomials of $\cos\theta$ do not represent well the dependence of S_1^1 on latitude. It is interesting to note that classic tidal theory also predicts slow decreases or secondary peaks of S_1^1 over the subtropics (Braswell and Lindzen 1998).

The amplitudes of waves at higher wavenumbers also decrease poleward but at a slower pace than that for S_1^1 (Fig. 7). Figure 7 shows that besides S_1^1 other westward propagating waves ($s > 1$) are stronger than the eastward propagating waves ($s < 0$) in the 20°–50°N zone, whereas waves at $s = -2$–-4 are slightly stronger than waves at $s = 3$–5 over southern low latitudes (0°–30°S).

b. The solar semidiurnal oscillation, S_2

1) GLOBAL DISTRIBUTIONS OF AMPLITUDE AND PHASE

The amplitude of S_2 (Fig. 8) is more homogeneous zonally than that of S_1 (cf. Fig. 3) and is largest (~1.0–1.3 mb) in the Tropics over South America, the eastern and western Pacific, and the Indian Ocean. Here S_2 generally decreases poleward with largest gradients in the subtropics. The amplitude is about 0.3–0.6 mb over middle and high latitudes. The land–sea differences at a given latitude are relatively small compared with S_1.

Figure 8 shows that the zone of maximum amplitude ($\geq$1.0 mb) of S_2 extends northward to about 20°N in DJF. This is in contrast to S_1 whose maximum-amplitude zone moves northward and southward in phase with the ITCZ. The amplitude is about 0.1–0.3 mb smaller in JJA than in DJF over the Tropics. Over midlatitudes, seasonal variations of S_2 are small, although S_2 is slightly weaker in JJA than in DJF over northern midlatitudes.

Compared with Haurwitz and Cowley (1973), Fig. 8 reveals more regional and zonal variations, although the magnitude of the amplitude is comparable over most of the areas. Figure 8 also shows maximum amplitudes of S_2 over the eastern tropical Pacific, where Haurwitz and Cowley (1973) had no data. Figure 8 is also consistent with the regional analyses of Trenberth (1977), Mass et al. (1991), and Kong (1995).

Figures 9, 3, and 8 show that although S_2 is generally stronger than S_1 over the oceans, S_1 is comparable to or stronger than S_2 over most land areas, expecially in summer and over high terrain such as the western United States and the Tibetan Plateau. During JJA, S_1 is substantially stronger than S_2 over all Northern Hemisphere land areas. This is in contrast to the conventional notion (based on analyses of limited data before the 1970s) that S_2 predominates over much of the globe, a paradox that the classic theory of atmospheric tides was developed to solve (Chapman and Lindzen 1970; Lindzen 1990).

Figure 10 shows that for annual pressure S_2 peaks around 1000 and 2200 LST (phase $\sigma_2 = 150°$) at low- and midlatitudes, which is in good agreement with Haurwitz (1956). The phase is noisy at high latitudes, because of few observations and weak tidal signals there. The phase of S_2 does not change substantially from season to season. The land–sea differences in the phase are small.

To compare with earlier estimates of S_2 of North

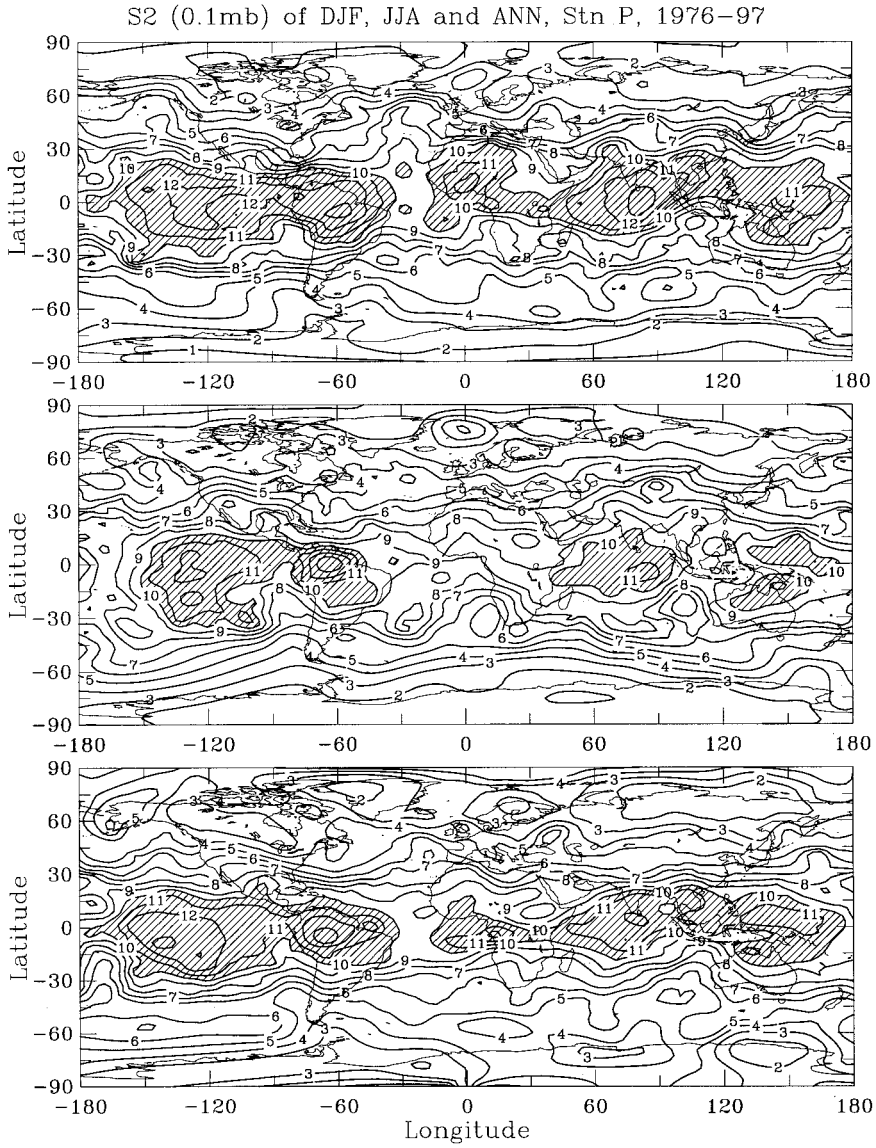

FIG. 8. Same as Fig. 3 except for the semidiurnal oscillation, S_2.

America (Spar 1952a; Hamilton 1980a,b) and the North Atlantic Ocean (Rosenthal and Baum 1956), which were derived using the data from the 1930s to the 1950s when pressure was likely to be measured by barometers different to those of recent decades, we plotted the amplitude and T_{max} of annual S_2 for the North Atlantic and North America domain (Fig. 11).

Comparison with Rosenthal and Baum (1956), who analyzed 3-hourly data from nine ship stations in the North Atlantic, revealed that our estimated amplitudes of S_2 are slightly higher (0.4 mb vs 0.3 mb) over the high-latitude Atlantic (50°–60°N) while the amplitudes are similar at the lower latitudes (35°–50°N, about 0.5–0.7 mb in winter and 0.4–0.5 in summer). However, our S_2 is less uniform zonally and increases slightly eastward in the North Atlantic. Rosenthal and Baum (1956) found a phase (T_{max}) of 0900–1100 LST for S_2 over the North Atlantic, which is comparable to Fig. 11. Based on the 1931–40 mean hourly pressure data from 100 U.S. stations, Spar (1952a) showed that the amplitude of annual S_2 decreases from about 0.8 mb at the southern border to about 0.3 mb at the northern border of the contiguous United States and the phase (T_{max} of annual S_2) is between 0930 and 1100 LST over the United States. Both the amplitude and phase are in good agreement with Fig. 11. Our S_2 over Canada (Fig. 11) is also comparable to earlier results of Hamilton (1980b), who analyzed 3-hourly surface data of 1951–60 from 60 Canadian stations, although our amplitude is slightly (by about 0.05–0.1 mb) higher than that of Hamilton (1980b). The above comparison suggests that instrumental errors associated with changes in barometers are

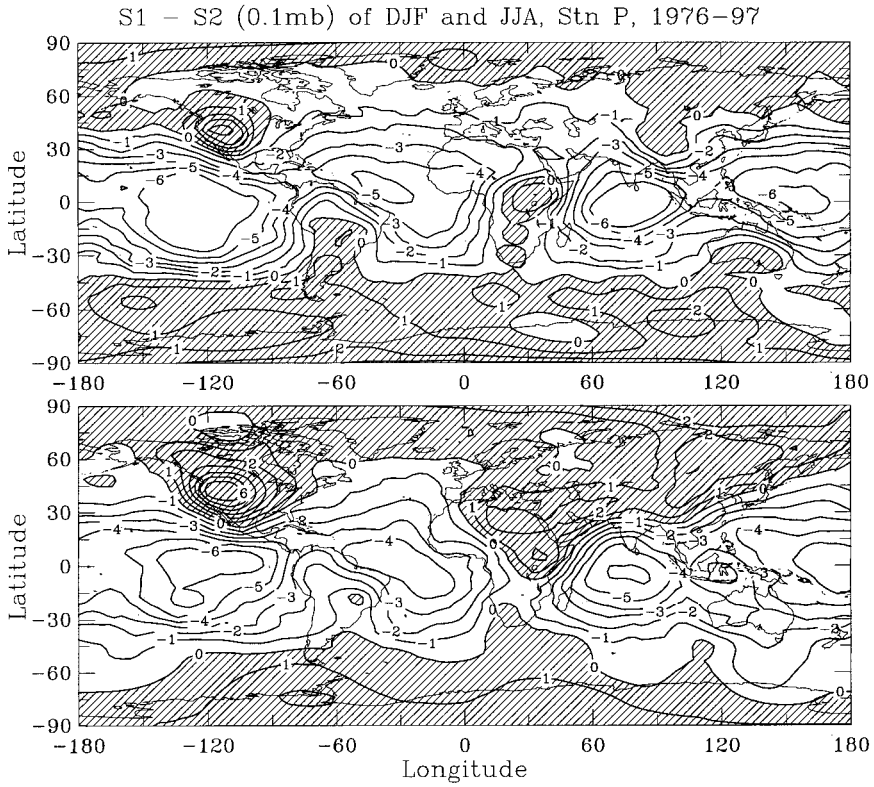

FIG. 9. Oscillation $S_1 - S_2$ difference in amplitude (in units of 0.1 mb) for DJF (upper panel) and (b) JJA (lower panel). Positive values are hatched.

likely to be relatively small and that surface pressure tides determined using the data of the recent decades are comparable to those based on the data before 1960.

2) ZONAL WAVE COMPONENTS

Figure 12 shows the globally averaged amplitudes for wave components at wavenumber $s = -13$ to $+15$ for DJF, JJA, and annual S_2. The wavenumber 2 component, S_2^2, has a global mean amplitude of about 566 μb in DJF, 523 μb in JJA, and 576 μb for annual mean, whereas the next closest amplitude is about 100 μb. The amplitudes at higher wavenumbers decrease only slightly. The seasonal differences in the wave components are small.

Figure 12 differs substantially from Haurwitz and

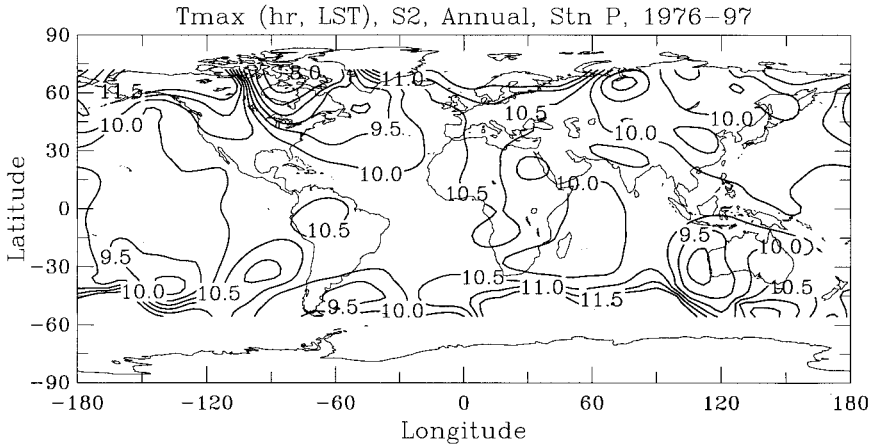

FIG. 10. Same as Fig. 4 except for S_2 and $S_2 = A_2 \sin(2\pi t/12 + \sigma_2)$, where $\sigma_2 = \pi/2 - 2\pi T_{max}/12$.

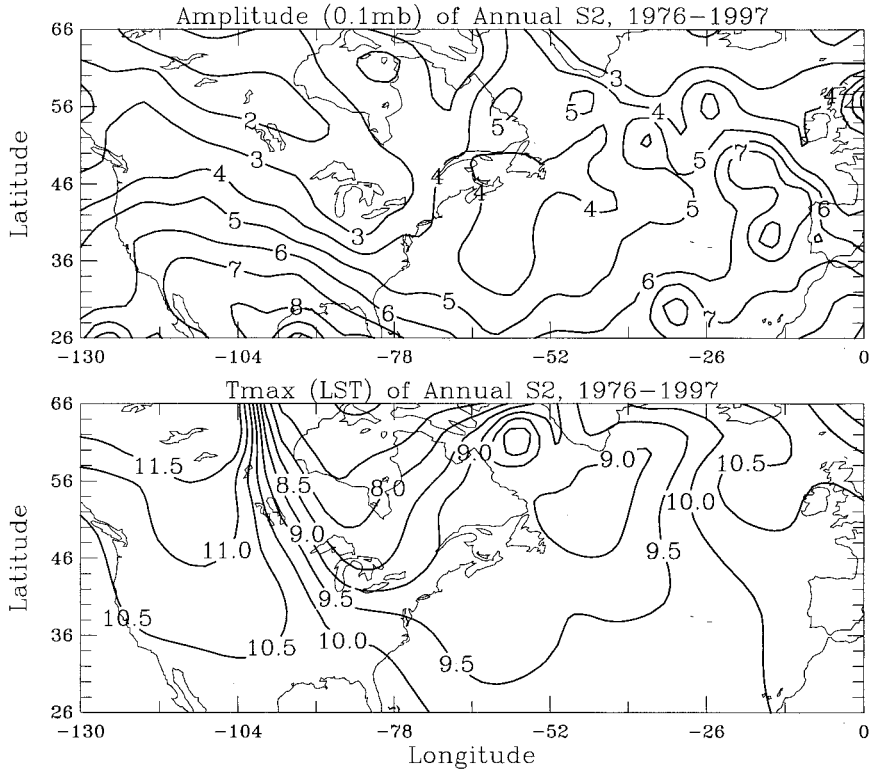

FIG. 11. Amplitude (0.1 mb) and phase (T_{max}, LST) of annual S_2 over North America and the North Atlantic Ocean.

Cowley (1973) in that their main wave S_2^2 is considerably stronger (≈750 μb for annual pressure) and their waves at $s \leq -1$ and $s \geq 4$ are much weaker (with amplitudes of 8–30 μb). This is expected because Haurwitz and Cowley (1973) had very limited spatial coverage, which could not resolve the higher wavenumber components and resulted in zonally homogeneous distributions.

The main wave S_2^2 for the annual S_2 has an amplitude of about 1096 μb around 4°N and it decreases rapidly to the north and south (Fig. 13). In the Tropics and northern subtropics, the DJF S_2^2 is stronger than the JJA S_2^2. From 40°S to 55°S, the amplitude increases poleward. Because of this, polynomials of $\cos\theta$ do not fit the curves well, and a function of $\cos^3\theta$, as used by Haurwitz and Cowley (1973), cannot represent the dependence of S_2^2 on latitude, expecially over middle and high latitudes.

Figure 14 shows that the amplitudes at higher wavenumbers also decrease poleward but at a much slower pace than that for S_2^2. The wave components are fairly symmetric relative to both the equator and wavenumber 2 for annual S_2.

c. S_1 *and* S_2 *in GEOS-1 reanalysis*

Figure 15 shows that the amplitude of annual S_1 in the GEOS-1 reanalysis is generally lower than observed over much of the globe except for the high-amplitude centers over South America, Africa, Australia, southern Asia, and the central tropical Pacific where the model has a positive bias. The zonal wave components of the assimilated S_1 are also dominated by S_1^1, but with a smaller global mean amplitude at $s = 1$ (≈330 μb for annual S_1^1) and considerably larger amplitude at $s = -3$ (≈156 μb) compared with the station data (cf. Fig. 5). The seasonal variations in the assimilated S_1 compare favorably with the station data. The assimilated S_1 peaks in the early morning (0400–0800 LST) over land areas and the Pacific, about 1–2 h earlier than the S_1 from station data (cf. Fig. 4).

The amplitude of S_2 in the reanalysis (Fig. 16) is more uniform zonally, about 0.2–0.5 mb larger at low latitudes, and about 0.1–0.3 mb smaller at high latitudes than observed (cf. Fig. 8). The assimilated S_2 is dominated by S_2^2, which has a global mean amplitude of 784 μb for annual pressure. This is considerably larger than that of Fig. 12 (576 μb). On the other hand, the amplitudes at higher wavenumbers for the assimilated S_2 are lower than observed, as expected from their smoother distributions.

Table 1 lists the migrating diurnal (S_1^1) and semidiurnal (S_2^2) tides of annual mean surface pressure along the equator estimated by various sources. It can be seen that both the GEOS-1 and NCEP–NCAR reanalysis data tend to overestimate the tides at the equator. Our esti-

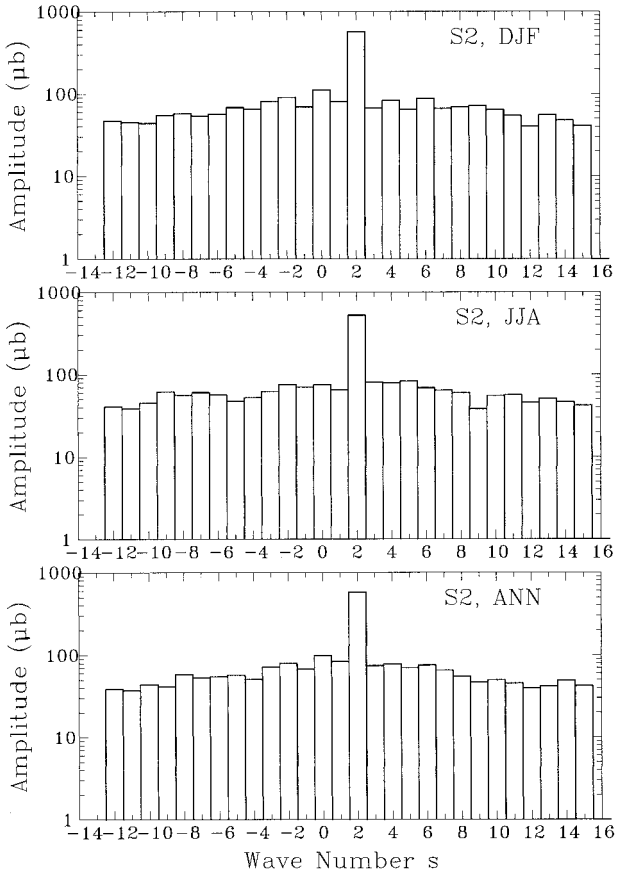

FIG. 12. Same as Fig. 5 except for S_2.

mates of S_1^1 and S_2^2 are similar to those of Haurwitz and Cowley (1973) around the equator, but the relative importance of S_1 increases at higher latitudes in our analysis.

5. Implications for the forcing of S_1 and S_2

Although sensible heating from the ground has been shown to be an important forcing for diurnal nonmigrating tides in model simulations (Tsuda and Kato 1989), it has not been included in classic tidal calculations (e.g., Chapman and Lindzen 1970; Braswell and Lindzen 1998). The fact that the amplitude of S_1 and its seasonal variations are much larger over the land than over the ocean suggests that over land areas S_1 is greatly enhanced by the sensible heating from the ground. Atmospheric total ozone concentrations are fairly uniform zonally over low and middle latitudes (McPeters et al. 1996) and water vapor contents are higher in marine air (Randel et al. 1996). Thus the solar absorption by ozone and water vapor cannot explain the land–sea differences in the amplitude of S_1. On average, the earth's surface absorbs about half of the incoming solar radiation at the top of the atmosphere (Kiehl and Trenberth 1997). Over land areas, the absorbed solar

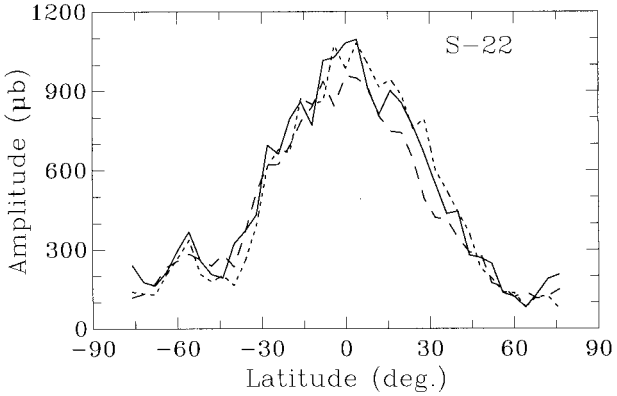

FIG. 13. Same as Fig. 6 except for S_2^2, the wavenumber 2 component of S_2.

radiation at the ground creates large sensible heating of the surface air and generates large diurnal ranges of surface air temperature (DTR) (Fig. 17; see also Dai et al. 1999b). On the other hand, because of the unlimited water for evaporation, the large specific heat of water, and the turbulence mixing in surface oceans, solar heating of the ocean surface does not provide strong sensible heating of marine surface air, resulting in much smaller DTR over the oceans than over land areas (Fig. 17). Indeed, the geographic variations of S_1 (Fig. 3) correlate significantly (attained significance level $p < 0.1\%$) with those of DTR (Fig. 17) (spatial correlation coefficient $r = 0.61$ for DJF, 0.67 for JJA, and 0.65 for annual mean). This is consistent with Mass et al. (1991), who found a correlation of 0.71 between summer diurnal amplitudes of surface pressure and DTR over the United States. Earlier studies also found stronger S_1 in clear sky and large DTR days than in cloudy and low DTR days in New York (Spar 1952b), but insignificant correlation between S_1 and DTR at a Bermuda maritime station (Haurwitz 1955).

Forced by the ozone and water vapor absorption of solar radiation, the classic tidal theory predicts a peak

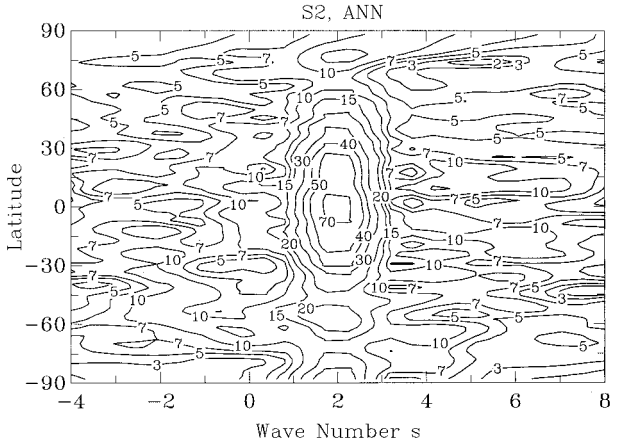

FIG. 14. Same as Fig. 7 except for S_2.

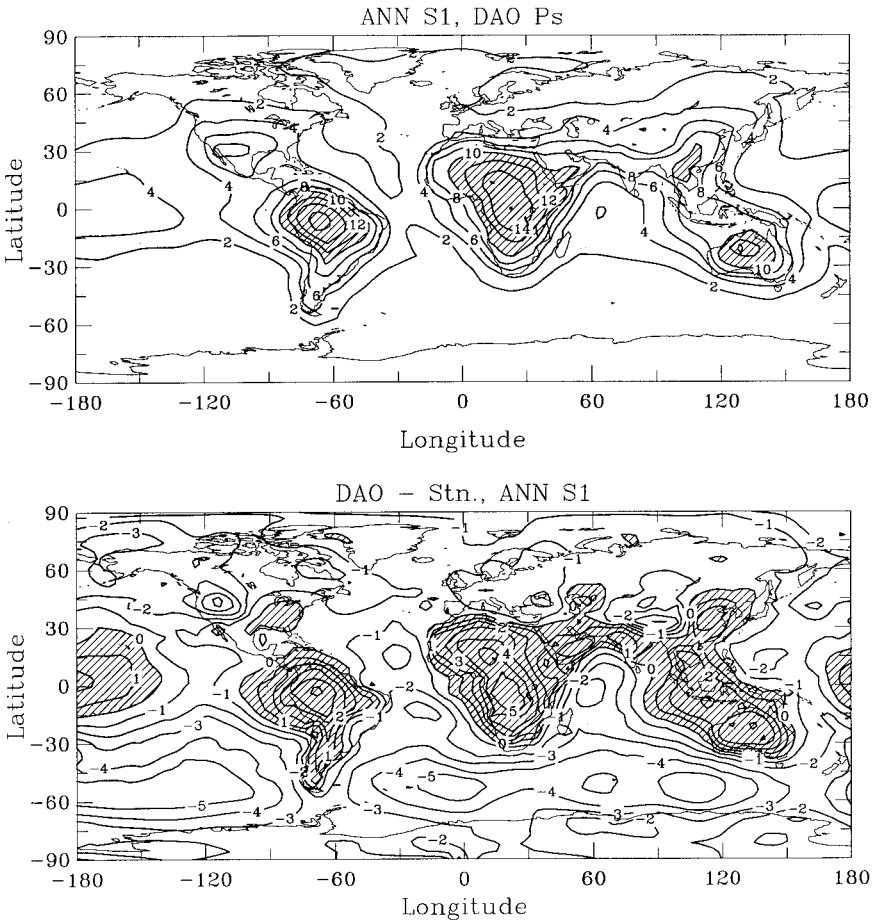

FIG. 15. Upper panel, amplitude (in units of 0.1 mb) of annual S_1 derived from the 1980–94 mean 3-hourly surface pressure field in the NASA GEOS-1 reanalysis. Values over 1.0 mb are hatched. Lower panel, the reanalysis minus observation difference of the amplitude (in units of 0.1 mb) of S_1. Positive values are hatched.

amplitude of 381 μb at the equator for annual S_1^1 (Braswell and Lindzen 1998), which is far below the observed (626 μb) (Table 1). Even with much weaker ground sensible heating than shown in Fig. 17, Tsuda and Kato (1989) showed through model simulations that large nonmigrating diurnal tides can be excited by the differential heating between land and ocean. Our results provide further evidence suggesting that sensible heat from the ground is a major forcing for both the migrating (S_1^1) and nonmigrating (S_1^s, $s \neq 1$) diurnal tides. Including this forcing in theoretical calculations should substantially reduce the gap between the theory-predicted and observed diurnal tides.

Although dominated by the migrating mode S_2^2, the semidiurnal tide S_2 exhibits considerable regional and zonal variations in its amplitude (cf. Fig. 8). For example, the amplitude of S_2 is smaller over the Atlantic and central Pacific than in other regions of the Tropics. Atmospheric water vapor content is comparable over the equatorial Pacific, Atlantic, and Indian Oceans and is much lower over Africa (Randel et al. 1996), while atmospheric total ozone concentration is fairly uniform over the Tropics (McPeters et al. 1996). Therefore, ozone and water vapor forcing appears unable to explain the variations of S_2 in the Tropics. Clouds, which can reflect (thus reducing the solar radiation reaching the lower troposphere where most of the water vapor absorption occurs) and absorb (thus providing additional forcing for S_2) solar radiation, are variable in space and could be a significant forcing for S_2. Precipitation has large diurnal variations (Dai et al. 1999a). The latent heating in convective precipitation is shown to be a significant forcing for S_2 in the Tropics (Lindzen 1978; Hamilton 1981). It could also induce additional zonal and regional variations in the amplitude of S_2. On the other hand, the sensible heating from the ground appears to have much smaller effects on S_2 than on S_1, as implied by the relatively small land–sea differences of S_2 (cf. Fig. 8). The signal of the influences by clouds and latent heating in S_2 is much weaker than that of the sensible heating in S_1. Therefore, a simple correlation between

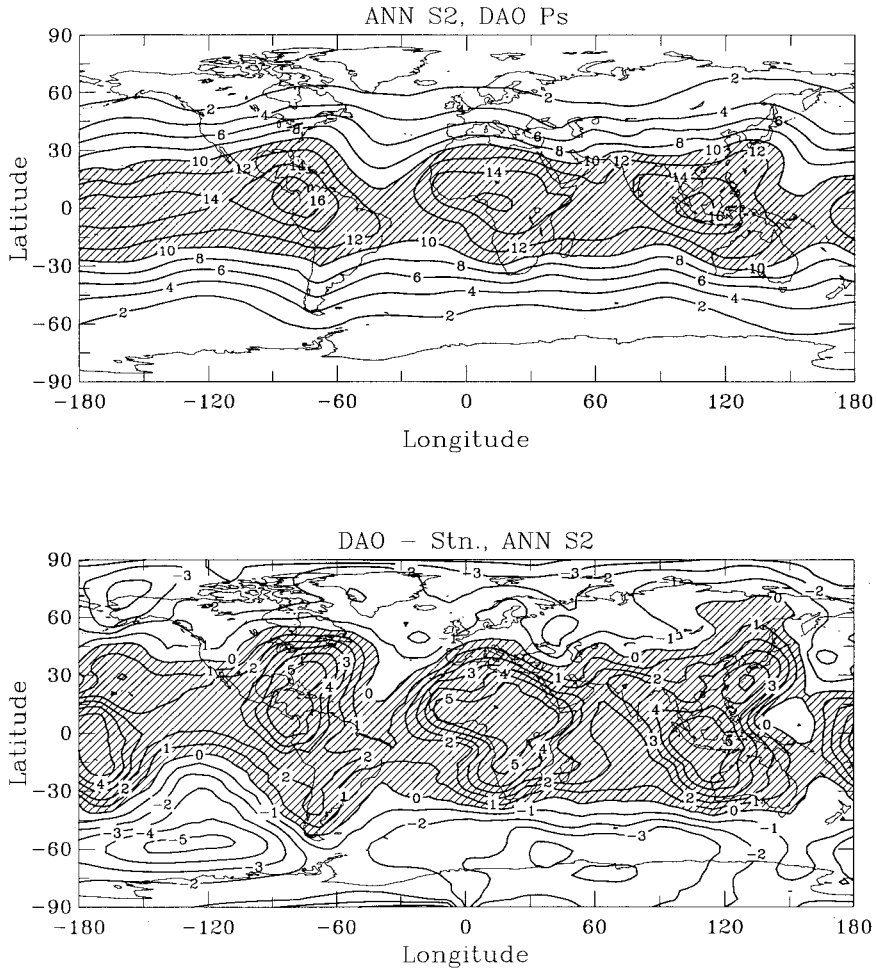

FIG. 16. Same as Fig. 15 except for S_2.

S_2 and cloudiness or convective precipitation is likely to result in weak relationships.

Figures 6 and 13 show that there is some asymmetry relative to the equator in the migrating tides. For example, the peak amplitude of S_1^1 is about 4° south of the equator. Furthermore, summer S_1^1 is substantially stronger than winter S_1^1 from about 20°N to 50°N. These features are not accounted for by the classic tidal theory with only ozone and water vapor heating (Braswell and Lindzen 1998).

TABLE 1. The amplitude (mb) of migrating diurnal (S_1^1) and semidiurnal (S_2^2) tides of annual-mean surface pressure along the equator estimated by various sources.

	Station data[a]	Station & marine data[b]	GEOS-1 reanalysis[b]	NCEP–NCAR reanalysis[c]	Classic theory
S_1^1	0.63	0.63[d]	0.71[d]	0.67	0.38[f]
S_2^2	1.16	1.10[e]	1.41[e]	1.47	1.10[g]

[a] From Haurwitz and Cowley (1973).
[b] This study.
[c] From van den Dool et al. (1997).
[d] Around 4°S.
[e] Around 4°N.
[f] From Braswell and Lindzen (1998).
[g] From Lindzen (1990).

6. Summary

Global surface pressure data of the 1976–97 period from over 7500 stations and COADS marine reports have been analyzed using harmonic and zonal harmonic methods. The spatial coverage of these data is greatly improved over previous similar analyses and is sufficient over most of the globe for capturing large-scale (>500 km) variations. However, the data are still sparse over the Antarctic, the Arctic, and the southern (south of about 50°S) oceans, where our results are less reliable.

We find that the diurnal pressure oscillation S_1 is comparable to the semidiurnal pressure oscillation S_2 in magnitude over much of the globe except for the low-latitude open oceans, where S_2 is about twice as strong as S_1. Over Northern Hemisphere land areas, S_1 is even stronger than S_2 during summer. Our results show that

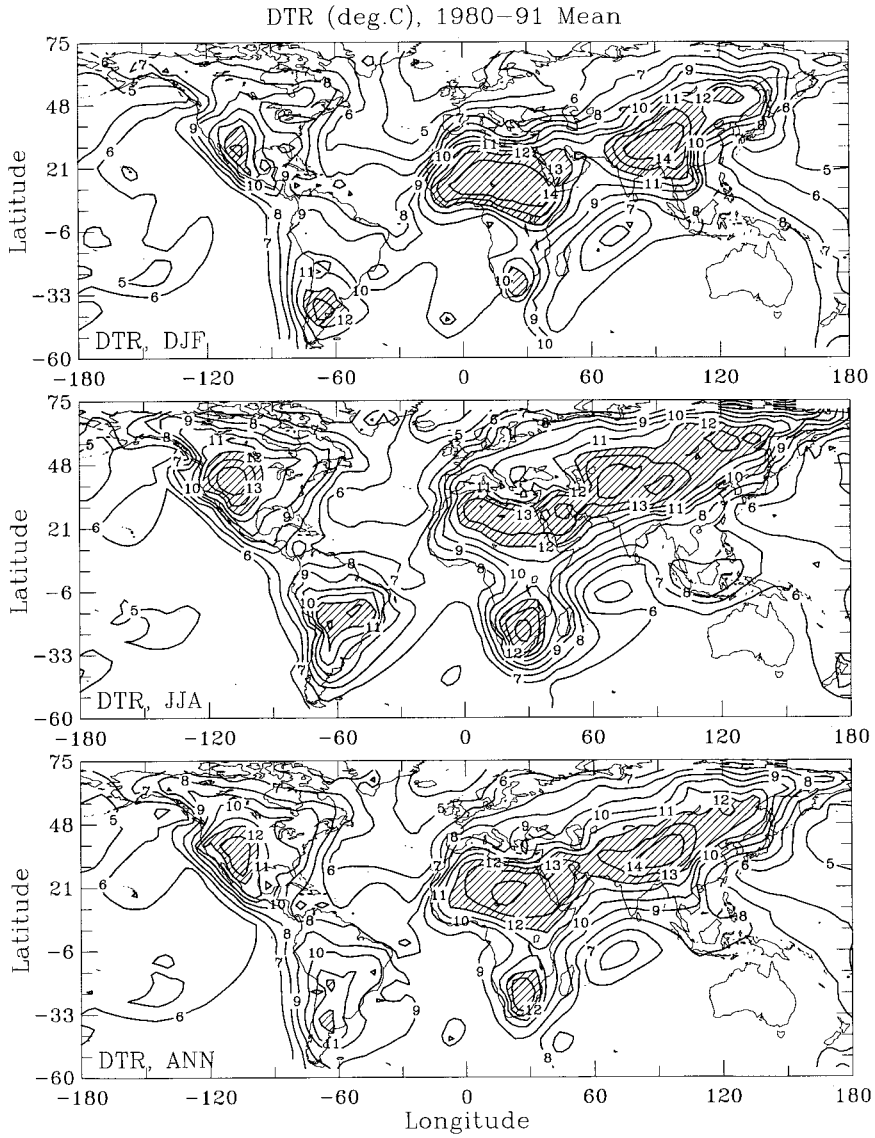

FIG. 17. Observed annual mean range of surface air temperature (°C) averaged over the 1980–91 period. Data are not available over Australia and sparse over the open oceans (Dai et al. 1999b).

S_1 is more important than previously thought (e.g., Chapman and Lindzen 1970; Lindzen 1990).

Compared with previous studies (Haurwitz 1956; Haurwitz 1965; Haurwitz and Cowley 1973), we find that there is much more variation in S_1 and S_2 on regional and continental scales, and that the nonmigrating tides are considerably stronger than previously reported. Oscillation S_1 is greatly influenced by landmasses and is generally stronger over the land than over the ocean. The highest amplitudes (~1.3 mb) of S_1 are found over northern South America and eastern Africa close to the equator. Here S_1 is also strong (~1.1 mb) over high terrain such as the Rockies and the Tibetan Plateau. Over the open oceans, the amplitude of S_1 is about 0.3–0.6 mb. Over land areas, S_1 is strongest in local summer as the solar heating reaches a maximum, whereas its seasonal variation over the oceans is small. At low latitudes S_1 reaches maxima in the morning around 0600–0800 LST, while it peaks in the late morning around 1000–1200 LST at midlatitudes except for eastern Asia and the North Pacific where the maximum is around 0600–0800 LST.

The wavenumber 1 component S_1^1 of S_1 has a global mean amplitude of about 370 μb, compared with the next strongest wave (S_1^2) of about 100 μb. The amplitude of S_1^1 decreases poleward rapidly at low latitudes, but its dependence on latitude cannot be adequately represented by simple polynomials of the cosine of latitude.

The largest amplitudes of S_2 (~1.0–1.3 mb) are found in the Tropics over South America, the eastern and western Pacific, and the Indian Ocean. The amplitude of S_2 is about 0.3–0.5 mb over middle and high latitudes. Land–sea differences at a given latitude in the amplitude of S_2 are much smaller than for S_1. The seasonal variations of S_2 appear to be out of phase with S_1. Specifically, the maximum-amplitude zone of S_2 extends northward to about 20°N in DJF while S_2 is weaker over low latitudes and northern midlatitudes in JJA. Here S_2 peaks around 1000 and 2200 LST at low- and midlatitudes.

Oscillation S_2 is dominated by its migrating (wavenumber 2) mode S_2^2, which has a global mean amplitude ranging from 523 (for JJA) to 566 (for DJF) μb, more than five times larger than the next strongest wave (~100 μb). Here S_2^2 peaks in the Tropics (about 958 μb for JJA and 1081 μb for DJF) and decreases rapidly poleward with a slower pace at mid- and high latitudes.

The amplitudes of high wavenumber components decrease gradually with increasing wavenumbers. We did not find any other wave components (except S_1^1 and S_2^2) that are substantially stronger than their adjacent ones. Low gridding resolution of S_1 and S_2 tends to reduce the amplitudes at higher wavenumbers and enhance S_1^1 and S_2^2.

The fact that the amplitude of S_1 and its seasonal variations are much larger over the land than over the ocean suggests that over land areas S_1 is greatly enhanced by the sensible heating from the ground. The spatial variations of the amplitude of S_1 correlate significantly with those in the diurnal temperature range at the surface, which is a proxy of the surface sensible heating. On the other hand, the land–sea differences of S_2 are relatively small, suggesting that the sensible heating from the ground has a much smaller influence on S_2. Although the amplitude of S_2 generally decreases poleward with largest gradients in the subtropics, there are considerable zonal variations that cannot be explained by zonal variations in atmospheric ozone and water vapor. Other forcings such as those through reflection and absorption of solar radiation by clouds and latent heating associated with convective precipitation are likely to be important for the zonal and regional variations in S_2. There is also some asymmetry relative to the equator in the migrating tides, especially S_1^1, which also implies additional forcings other than the solar heating by atmospheric ozone and water vapor.

Acknowledgments. We are grateful to Steve Worley for assisting us with the COADS dataset, Gregg Walters for his help with the GTS station dataset, and Dennis Shea for computer assistance. We thank Kevin Trenberth for his constructive comments, Clara Deser for suggesting the zonal shift of the marine pressure data, and Roland Madden for reading an earlier version of the manuscript. We also thank the three anonymous reviewers for their careful reading of the manuscript and many constructive comments, which resulted in the addition of Table 1 and Fig. 11. Dai was supported by a NOAA Postdoctoral Program in Climate and Global Change fellowship, administered by the University Corporation for Atmospheric Research. J. Wang is supported by National Science Foundation Grant ATM-9223150.

REFERENCES

Braswell, W. D., and R. S. Lindzen, 1998: Anomalous short wave absorption and atmospheric tide. *Geophys. Res. Lett.,* **25,** 1292–1296.

Chapman, S., and R. S. Lindzen, 1970: *Atmospheric Tides.* D. Reidel, 200 pp.

Cooper, N. S., 1984: Errors in atmospheric tidal determination from surface pressure observations. *Quart. J. Roy. Meteor. Soc.,* **110,** 1053–1059.

Dai, A., and C. Deser, 1999: Diurnal variations in global surface wind fields. *J. Geophys. Res.,* in press.

——, F. Giorgi, and K. E. Trenberth, 1999a: Observed and model simulated precipitation diurnal cycle over the contiguous United States. *J. Geophys. Res.,* **104**, 6377–6402.

——, K. E. Trenberth, and T. R. Karl, 1999b: Effects of clouds, soil moisture, precipitation and water vapor on diurnal temperature range. *J. Climate,* **12**, 2451–2473.

Deser, C., and C. A. Smith, 1998: Diurnal and semidiurnal variations of the surface wind field over the tropical Pacific Ocean. *J. Climate,* **11,** 1730–1748.

Forbes, J. M., and H. B. Garrett, 1979: Theoretical studies of atmospheric tides. *Rev. Geophys. Space Phys.,* **17,** 1951–1981.

Groves, G. V., and A. Wilson, 1982: Diurnal, semi-diurnal and terdiurnal Hough components of surface pressure. *J. Atmos. Terr. Phys.,* **44,** 599–611.

Hamilton, K., 1980a: Observations of the solar diurnal and semidiurnal surface pressure oscillations in Canada. *Atmos.–Ocean,* **18,** 89–97.

——, 1980b: The geographical distribution of the solar semidiurnal surface pressure oscillation. *J. Geophys. Res.,* **85,** 1945–1949.

——, 1981: Latent heat release as a possible forcing mechanism for atmospheric tides. *Mon. Wea. Rev.,* **109,** 3–17.

Haurwitz, B., 1955: The thermal influence on the daily pressure wave. *Bull. Amer. Meteor. Soc.,* **36,** 311–317.

——, 1956: The geographical distribution of the solar semi-diurnal pressure oscillation. *New York Univ. Coll. Eng. Meteor. Pap.,* **2** (5), 1–36.

——, 1965: The diurnal pressure oscillation. *Arch. Meteor. Geophys. Bioklimat. A,* **14,** 361–379.

——, and D. Cowley, 1973: The diurnal and semidiurnal barometric oscillations, global distribution and annual variation. *Pure Appl. Geophys.,* **102,** 193–222.

Hsu, H.-H., and B. Hoskins, 1989: Tidal fluctuations as seen in ECMWF data. *Quart. J. Roy. Meteor. Soc.,* **115,** 247–264.

Janowiak, J. E., P. A. Arkin, and M. Morrissey, 1994: An examination of the diurnal cycle in oceanic tropical rainfall using satellite and in situ data. *Mon. Wea. Rev.,* **122,** 2296–2311.

Kiehl, J. T., and K. E. Trenberth, 1997: Earth's annual global mean energy budget. *Bull. Amer. Meteor. Soc.,* **78,** 197–208.

Kong, C.-W., 1995: Diurnal pressure variations over continental Australia. *Aust. Meteor. Mag.,* **44,** 165–175.

Lindzen, R. S., 1967: Thermally driven diurnal tide in the atmosphere. *Quart. J. Roy. Meteor. Soc.,* **93,** 18–42.

——, 1978: Effect of daily variations of cumulonimbus activity on the atmospheric semidiurnal tide. *Mon. Wea. Rev.,* **106,** 526–533.

——, 1979: Atmospheric tides. *Ann. Rev. Earth Planet Sci.,* **7,** 199–225.

——, 1990: *Dynamics in Atmospheric Physics.* Cambridge University Press, 310 pp.

Mass, C. F., W. J. Steenbergh, and D. M. Schultz, 1991: Diurnal surface-pressure variations over the continental United States and the influence of sea level reduction. *Mon. Wea. Rev.,* **119,** 2814–2830.

McPeters, R. D., and Coauthors, 1996: Nimbus-7 Total Ozone Mapping Spectrometer (TOMS) Data Products User's Guide. NASA Ref. Publ. 1384, Goddard Space Flight Center, Greenbelt, MD.

Randel, D. L., T. H. Vonder Haar, M. A. Ringerud, G. L. Stephens, T. J. Greenwald, and C. L. Combs, 1996: A new global water vapor dataset. *Bull. Amer. Meteor. Soc.,* **77,** 1233–1246.

Rosenthal, S. L., and W. Baum, 1956: Diurnal variation of surface pressure over the North Atlantic Ocean. *Mon. Wea. Rev.,* **84,** 379–387.

Spar, J., 1952a: Characteristics of the semidiurnal pressure waves in the United States. *Bull. Amer. Meteor. Soc.,* **33,** 438–441.

——, 1952b: The thermal influence on the daily pressure wave. *Bull. Amer. Meteor. Soc.,* **33,** 339–343.

Trenberth, K. E., 1977: Surface atmospheric tides in New Zealand. *New Zealand J. Sci.,* **20,** 339–356.

——, and C. J. Guillemot, 1994: The total mass of the atmosphere. *J. Geophys. Res.,* **99,** 23 079–23 088.

——, J. W. Hurrell, and A. Solomon, 1995: Conservation of mass in three dimensions in global analyses. *J. Climate,* **8,** 692–708.

Tsuda, T., and S. Kato, 1989: Diurnal non-migrating tides excited by a differential heating due to land–sea distribution. *J. Meteor. Soc. Japan,* **67,** 43–55.

van den Dool, H. M., and S. Saha, 1993: On the seasonal redistribution of mass in a 10-yr GCM run. *J. Climate,* **6,** 22–30.

——, ——, J. Schemm, and J. Huang, 1997: A temporal interpolation method to obtain hourly atmospheric surface pressure tides in reanalysis 1979–1995. *J. Geophys. Res.,* **102,** 22 013–22 024.

Wallace, J. M., and F. R. Hartranft, 1969: Diurnal wind variations, surface to 30 kilometers. *Mon. Wea. Rev.,* **97,** 446–455.

Watson, D. F., 1994: *nngridir: An Implementation of Natural Neighbor Interpolation.* 170 pp. [Available from David Watson, P.O. Box 734, Clavemont, WA 6010, Australia.]

Whiteman, C. D., and X. Bian, 1996: Solar semidiurnal tides in the troposphere: Detection by radar profiles. *Bull. Amer. Meteor. Soc.,* **77,** 529–542.

Woodruff, S. D., S. J. Lubker, K. Wolter, S. J. Worley, and J. D. Elms, 1993: Comprehensive ocean-atmosphere data set (COADS) release 1a: 1980–1992. *Earth System Monitor,* **4** (1), 1–8.

Wu, J., A. da Silva, and S. Schubert, 1997: Fifteen years (1980–1994) of three hourly surface pressure from GEOS-1 Reanalysis. Tech. Note. Data Assimilation Office, NASA Goddard Space Flight Center, Greenbelt, MD.